Determination of interface roughness and its correlation in amorphous-silicon/ amorphous-germanium multilayers

Victor M. Pantojas
Assistant Professor, PUPR

Abstract

The importance of surfaces and interfaces of materials is increasing in many technological areas. In the microelectronic industry, for example, the current trend is toward even faster and smaller electronic devices. Devices such as metal-oxide semiconductor field effect transistors (MOSFET) function by manipulating the density of electrons trapped in a potential well at the oxide-semiconductor interface. The insulator-semiconductor interface will play an increasingly important role in the performance of this and similar devices. A clear understanding of the role played by the interface and how the interface morphology may affect the device performance is necessary. The possibility of constructing multilayered structures, which increase the interface to volume ratio, has opened a number of possibilities in the study of interface morphology and its relation with growth.

In this work I study surface and interface roughness in hydrogenated amorphous-silicon/ amorphous-germanium multilayers by means of x-ray scattering techniques. Specular and diffuse x-ray scattering measurements were performed in order to study how roughness propagates from interface to interface during growth, as well as to examine the lateral length scale of the roughness, which is related to the surface diffusion process. Interface roughness was found to increase sub-linearly with distance of the interface from the substrate. The root mean square roughness near the substrate was found to be about 0.3 nm whereas at the surface the best fit was found for 1.8 nm of rms roughness. It was found that interface roughness was highly correlated from layer to layer and a correlation length of 30 nm was obtained.

The fact that roughness is correlated from interface to interface on a scale given by the correlation length suggests that lateral diffusion during growth was of order, of or below, 30 nm.

Sinopsis

Determinación de la aspereza de interfase y su correlación en multicapas de silicio amorfo - germanio amorfo

La importancia de la superficie de los materiales, al igual que la interfase entre diferentes materiales, ha aumentado significativamente en muchos aspectos tecnológicas. En la industria microelectrónica, por ejemplo, la tendencia actual es hacia el diseño de componentes electrónicos cada vez mas rápidos y pequeños. El transistor llamado MOSFET, que se compone de tres capas, metal/óxido/semiconductor, funciona manipulando la densidad de electrones atrapados en el pozo de energía potencial que crea la interfase entre el óxido y el semiconductor. La perfección de interfaces como éstas determinará la calidad de los transistores al igual que de muchos otros dispositivos electrónicos. Por esta razón es necesario saber cómo la morfología de la interfase afecta el funcionamiento del dispositivo. Adelantos recientes en la tecnología de crecimiento de películas finas sobre substratos ha hecho posible crear estructuras de muchas capas con un gran número de interfaces, lo cual aumenta las posibilidades en el estudio de la morfología de interfaces y su relación con el crecimiento.

En este trabajo se estudia la aspereza de la superficie y las interfaces en capas múltiples (100 capas) de silicio amorfo hidrogenado y germanio amorfo hidrogenado con técnicas de difracción de rayos x. Se tomaron medidas de la difracción especular y difusa de rayos x para estudiar cómo la aspereza se propaga de interfase en interfase durante el crecimiento y cuál es su escala de longitud lateral, la cual está relacionada con el proceso de difución superficial. Encontramos que la aspereza de la interfase aumenta de una manera sublineal con la distancia de la interfase al substrato. Cerca del substrato el valor rms de la aspereza fue de 0.3 nm mientras que en la superficie se observó un valor de 1.8 nm. Se encontró que la aspereza de las interfaces estaba altamente

correlacionada de interfase al interfaz con una longitud de correlación de 30 nm. Esto sugiere que la difución lateral durante crecimiento fue de menos de 30 nm.

Introduction

That amorphous multilayers deposited by plasma enhanced vapor deposition with precise control over layer repeat distance and interface quality was first demonstrated in 1983 (Abeles and Tiedje, 1983). Since then a number of investigators have studied the properties of this new type of material. Their optical and electronic properties (Wronnki et al., 1986; Shirai et al., 1986), their application to solar cells (Tsuda et al., 1987), and their properties as photoreceptors (Shirai et al., 1986) have been studied. In addition, quantum size effects in ultra-thin a-Si:H/a-Ge:H multilayers (Persans et al., 1985) and a-Si:H/a-SiN:H multilayers have been reported. Many of these properties are strongly linked to the interface between the layers. Therefore, the degree of perfection of the interfaces between the different materials can significantly affect these properties. Several techniques have been used to characterize interfaces including Raman scattering (Maley et al, 1985) (Williams et al, 1988) and cross-sectional transmission electron microscopy (Lepetre et al., 1987). Small-angle x-ray reflectivity, which is commonly used to study multilayer x-ray mirrors (Nevot and Croce, 1980; Spiller, 1988; Stearn, 1989), has only recently been used to study amorphous multilayers (Miyazaki et al.,1988; Persans et al., 1989).

In this work I characterize interface roughness and roughness correlation by modeling the specular and diffuse x-ray reflectivity. The specular reflectivity will give information about the average interface roughness in the multilayer whereas the amount and distribution of the diffuse scattering is related to the lateral scale of the roughness and the way in which roughness correlates from interface to interface. Knowledge of the magnitude of the interface roughness, its lateral scale, and the way in which roughness from one interface relates to roughness in another interface will lend insight into the fundamental process involved in film growth. In the simplest case, the

evaporative deposition of material onto a clean substrate, roughness arises from the competition between the arrival rate of the depositing species and its lateral surface diffusion rate. Interface roughness is also expected to depend on the film thickness since the growth process can be stopped at any stage. In the case where more than one material with different properties are grown on a substrate, interface roughness can be the result of different growth mechanisms. Asymmetric roughening can also take place, where the roughness profile can be different .depending on what material is grown on top. For example, if a heavy element is deposited on top of a lighter element in a ballistic way then the roughness profile can differ from the case where the lighter element is deposited on top of the heavy one. Finally, interdiffusion or chemical reactions between the deposited layers can take place, creating a rough mixed layer.

Understanding the relationship between growth processes and roughness correlation is needed if one is to ultimately control roughness in multilayer devices. The use of diffuse x-ray reflectance to study roughness correlation in multilayers was developed in 1991 (Savage et al., 1991) and used in the study of W/C x-ray mirrors. We will use this technique to analyze these newly developed amorphous multilayers.

X-ray reflectivity simulation

Specular reflectivity

For a single surface, roughness is known to cause angular broadening of the intensity distribution of the reflected light. Thus, roughness reduces the amount of light specularly reflected while increasing the diffusely scattered light. Experimental evidence of the effect of roughness on x-ray reflectivity from a single surface was presented by Ehrenberg (1949) while working with grazing angle mirrors for x-ray imaging. He suggested that surface roughness can be described by a Fourier series of spatial wavelengths and demonstrated that mirror surfaces must be polished to an extremely low level of surface roughness in order to provide an acceptable image. The need for extremely smooth surfaces for x-ray mirrors prompted a number of experimental studies

on flat samples with different materials and polishing methods. Some of the experiments were compared with the electromagnetic scattering theories previously developed for optical scattering. The applicability of these theories to the x-ray regime is questionable because they are only valid when the wavelength of the light is much longer than the rms roughness.

A different approach was taken by Nevot and Croce (1980) with a model that treats roughness as a gradual change in the index of refraction of the material. More recently Sinha et al. (1988) introduced a model based on the scalar theory in the Born approximation. Their result for the effect of roughness on the specular reflection is consistent with that obtained by L. Nevot and P. Croce. In both theories the expression for the specular reflection is given by:

$$I_{spec} = I_0 \, e^{-8\pi^2\sigma^2 q_z q_z^t} \qquad (1)$$

where σ is the rms roughness, q_z and q_z^t are the normal components of the incident and scattered wave-vectors. This result is valid for a Gaussian distribution of surface heights and small $q\sigma$ product. The exponential in this equation has the effect of attenuating the reflectivity as either roughness or the perpendicular component of the wave-vector (i.e. diffraction order) is increased. This exponential is known as the "static" Debye-Waller factor because it is similar the well known Debye Waller factor resulting from the disorder caused by thermal vibration.

A more complicated problem arises when we consider the case of multilayers where roughness from buried interfaces affects the reflectivity and multiple scattering has to be considered. Therefore, when analyzing multilayers it is important to know how roughness correlates from interface to interface. This is achieved by the introduction of a "cross-correlation" function which compares the roughness profiles of two interfaces. A cross-correlation length will then describe how a given surface feature is reproduced from interface to interface.

The treatment of interface roughness and its effect on reflectivity can be greatly simplified if one considers two extreme cases. Suppose that each deposited layer completely reproduces the roughness profile of the previous layer without smoothing or adding any roughness. In this case we have "complete correlation," which simplifies the problem because we can characterize the multilayer roughness by an effective single layer profile and the resultant reflectivity will be given by the product of the intensity scattered by a single rough surface and the reflectivity of the perfect multilayer. The other extreme case, when roughness from the interfaces is completely "uncorrelated" or random, the total reflectivity will be given by the incoherent sum of the intensities diffusely scattered from each interface plus the reduced specular reflectivity.

In real multilayers neither case is expected to be true. From optical scattering studies of coatings it is observed that overlayers often replicate the roughness profile of the substrate for long spatial surface waviness while the short ones appear to be random (Harvey et al., 1989). In this case interface roughness can be separated into two parts, one which is due to the short spatial random roughness, also called the intrinsic roughness, and one due to the correlated roughness replicated from interface to interface such that

$$\sigma^2 = \sigma_c^2 + \sigma_{int}^2 \quad (2)$$

The effects of these two types of roughness on the total reflectivity are distinct and their separate contributions can be obtained from the correct set of measurements. For perfect correlation, for example, the diffuse intensity along q_z will be peaked at the Bragg condition, $q_z = 2\pi n/d$ similar to the specular reflectivity. For vertically random roughness, the diffuse intensity will not be peaked, but will be spread out uniformly in q_z.

The total rms roughness can be obtained by fitting the specular reflectivity as a function of q_z. For this we use a dynamic approach to computing the x-ray reflectivity for the multilayer. This approach is based

upon the recursive computation using Fresnel reflection coefficients (Parrat, 1954). We characterize a material by its complex refractive index: $n=1-\delta-i\beta$. In the x-ray regime δ and β are small and positive, of order 10^{-5} and 10^{-6} respectively. As an example, the Fresnel coefficient for s-polarized light for the interface between the j and the j + 1 layers is:

$$F_{j,j+1} = \frac{g_j - g_{j+1}}{g_j - g_{j+1}} C \qquad (3)$$

where $g_j = (n_j^2 - \cos^2\theta)^{1/2}$. We have introduced the Debye Waller factor C to account for interface roughness. The reflectivity of the multilayer is computed by recursion from the substrate film interface in the following manner. We define $R_{j,j+1} = a_j(E_j^R/E_j)$ and $a_j = \exp(-i\pi g_j d_j/\lambda)$ where d_j is the layer thickness and E_j^R is the reflected wave amplitude. The recursion relation (eq. 4) is then used to compute the reflected intensity, $I(\theta)/I_0 = R_{1,2}\,R_{1,2}^*$.

$$R_{j,j+1} = a_j^4 \frac{[R_{j+1,j+2} + F_{j,j+1}]}{[R_{j+1,j+2}F_{j,j+1} + 1]} \qquad (4)$$

Diffuse reflectivity

Information on the lateral length scale of the surface and interface roughness can be obtained from measurements of the angular distribution of diffusely scattered x rays. For a single rough surface the shape of the diffuse intensity reflects the scattering by the various Fourier components that the roughness represents and the strength of these components. Lateral correlation is introduced in the height-heigth correlation function and both Gaussian and exponential correlation functions have been used to model surface roughness. More recently attempts to treat the rough surface as a fractal have given rise to other choices (Sinha et al., 1988). In this work we will use the expression

for the scattered intensity of a single surface derived by S. Sinha et al. (1988), which for an exponential correlation function can be evaluated analytically:

$$I(q_x,q_z) = \left\{\frac{2\pi I_0(e^{-q_z^2\sigma^2})}{q_z^2}\right\}\left\{2\pi\delta(q_x)+\frac{\sum^{m-\infty} 2\varsigma(q_z^2\sigma^2)^m}{[m(m!)(1+q_x^2\varsigma^2/m^2)]}\right\} \quad (5)$$

where ζ is the correlation length, q_x and q_z are the x and z components of the wave vector $|q| = 2\pi/\lambda$ and σ is the roughness. The intensity distribution can be separated in two terms, a delta function which represents the specular reflection, and the diffuse term, which is represented by a sum of Lorentzians. In general the area under the diffuse component depends on the rms roughness, while the width is inversely related to the correlation length ς. More complicated correlation functions can be used but the intensity can be obtained only with numerical methods. Thus, fitting the shape of the reflected peaks in q_x with the model for a single surface will give the rms roughness and lateral correlation length for completely vertically correlated roughness.

Sample preparation

Amorphous Si/Ge multilayers were deposited by low-pressure plasma-assisted chemical vapor deposition from pure SiH_4 and H_4/GeH_4 in the ratio 10:1 respectively. Periodic multilayers were obtained by periodically alternating the gases in the growth chamber. The switching of the gases was computer controlled. The growth rate of the a-Si:H and a-Ge:H was about 0.1 nm/s and the gases can be exchanged in the deposition chamber within one second with the accuracy in switching time of about 0.1 s. The samples were deposited on the 200^0 C anode of an rf diode deposition system. Other factors such as bias voltage, rf power, temperature, gas pressure and flow rate may influence growth rate; therefore, actual layer reproducibility may not be ideal.

Multilayer samples were deposited on fused silica substrates selected for low surface roughness. Samples were about 1 cm x 1 cm, cut from the center of a 5-cm diameter substrate. Macroscopic film thickness uniformity was found to be better than 5 % over a 1cm^2 area by measuring transmission interference fringes in the near infrared. The growth rate, as measured by in-situ optical reflectivity, varied by less than two percent over the two-hour growth time for a sample.

X-ray diffraction measurements

Reflectivity measurements were carried out on a 2.2 kW fixed Cu anode x-ray source. The goniometer was built with independent movement of θ (angle between source and sample) and 2θ (angle between source and detector). Rotation was achieved with the use of high precision digital micrometers with a step resolution of 1μm which were connected to computer-controlled stepping motors. The angular resolution with this arrangement was 0.001 degrees. The x-ray beam was collimated with a 65μm x 1cm slit at 23 cm from the source. The in-plane resolution was 0.016 degrees FWHM. The out-of-plane resolution was approximately 2 degrees, and the beam size at the axis of rotation of the goniometer was 0.2 mm by 3 cm. The detector was a scintillator and photomultiplier tube with a graphite crystal monochromator set to detect Cu K_α radiation ($\lambda = 0.154$ nm).

In order to separate the correlated and uncorrelated roughness we must first determine the true specular reflectivity. This is achieved in the (θ, 2θ) scan, which measures the specular reflectivity as a function of incident angle or depth. The reflectivity measured in this type of scan will have contributions from the diffuse scattering due to correlated roughness. Thus, the true reflectivity is obtained by subtracting this contribution. In an offset (θ, 2θ) measurement the crystal is rotated by an offset angle in order to measure the diffuse reflectivity as a function of incident angle. The true reflectivity will be the difference between these two profiles. Finally, we do a rocking curve measurement in which the detector is fixed while the crystal is rotated. This type of measurement profiles the angular distribution of the scattered intensity in the plane parallel to the surface. This angular distribution will give

information on the lateral length scales of the correlated roughness. Figure 1 shows the scattering geometries used in this work.

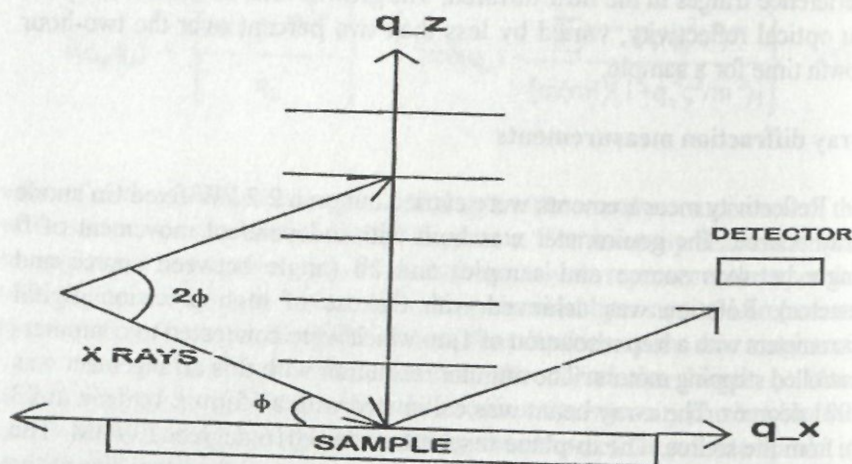

Figure 1: Reciprocal space representation of the scattering geometry

Experimental results and analysis

Specular reflectivity

The specular reflectivity [(θ, 2θ)-scan] for a 50 layer-pair multilayer is shown in the top curve of figure 2. The bottom curve in figure 2 shows the same type of measurement except that the sample is offset by 0.05° in order to scan the diffuse scattering as a function of depth. Figure 3 represents the true specular reflectivity for the multilayer. The intensity is plotted in a Log scale as a function of the z-component of the wave vector q_z. Reflectivity curves are characterized by a high reflectivity region bellow the critical angle, which for this sample is about 0.23 degrees. Above the critical angle the reflectivity falls off rapidly. For this sample the background falls more than four orders of magnitude and then levels off. The amount of the intensity drops

after the critical angle is related to the total interface roughness. On top of the falling background three distinctly shaped and spaced diffraction peaks are observed. Smaller periodic oscillations and intensity variations between peaks are also observed. The total number of oscillations between peaks will depend on the total number of layers.

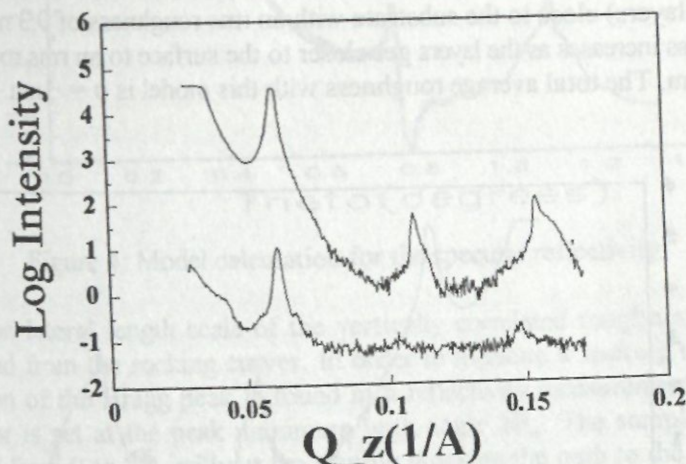

Figure 2. Top: Specular reflectivity(θ- 2θ) of a-Si:H/a-Ge:H multilayer with 100 layers. Bottom: Offset-specular reflectivity.

The angular position of the diffraction peaks is used in Bragg's equation $m\lambda = 2d_r \sin\theta_m$ modified to account for the deviation of the index from unity and the fact that the sample consists of layers of different indexes of refraction. The bilayer thickness or repeat distance was found to be $d_r = 11.8$ nm. From the second order peak, which should vanish if the Si and Ge layers have the same thickness, we found that the Si layer is about 3% bigger than the Ge layer. The best fits were found with $d_{Si} = 6.13$ nm and $d_{Ge} = 5.67$ nm. Using these parameters and assuming that densities of the materials are close to that of bulk, we modeled the multilayer reflectivity. The Debye-Waller factor which is used to model the effect of roughness allows for a roughness parameter at each interface. Figure 4 shows the result of the modeling. The matching of the features of the data with the dynamical parameters forces us to have a

relatively narrow set of roughness parameters and its profile as a function of depth. The fast drop of the reflectivity just above the critical angle suggests that the surface is rough(σ = 1.6-2 nm). The relative flatness of the region between peaks at large angles indicates that there are a set of relatively smooth interfaces close to the substrate. Thus, the roughness profile that best fits the data is one in which there are a set of smooth layers (estimated to be between 6 to 10 layers) close to the substrate with an rms roughness of 0.3 nm while roughness increases as the layers get closer to the surface to an rms roughness of 1.8 nm. The total average roughness with this model is σ = 1nm.

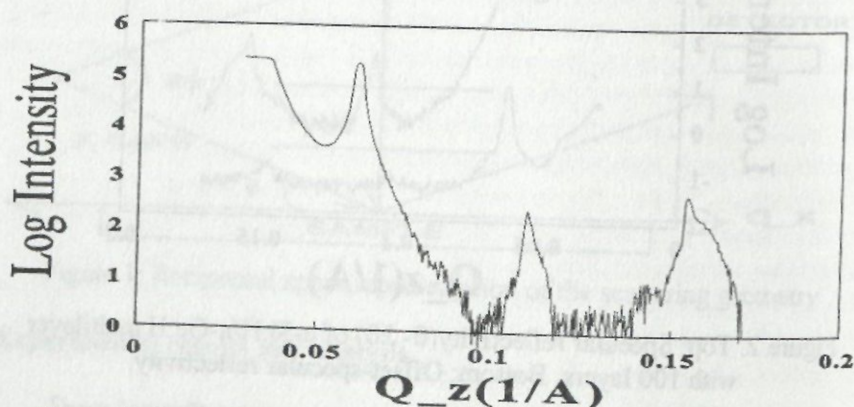

Figure 3. True specular reflectivity given by the distance between the reflectivity (θ - 2θ) measurement and the offset relectivity measurement

Diffuse reflectivity

The offset (θ, 2θ) measurement in the bottom graph of figure 2 shows that the diffuse reflectivity is peaked at the same Bragg angle as the specular reflectivity. This implies that vertically correlated roughness is present. Uncorrelated roughness should produce diffuse reflectivity away from the Bragg peaks. In this sample the amount of diffuse scattering between peaks appears to be negligible and most of the scattering can be assumed to be caused by correlated roughness. Therefore, roughness is mostly correlated

from interface to interface.

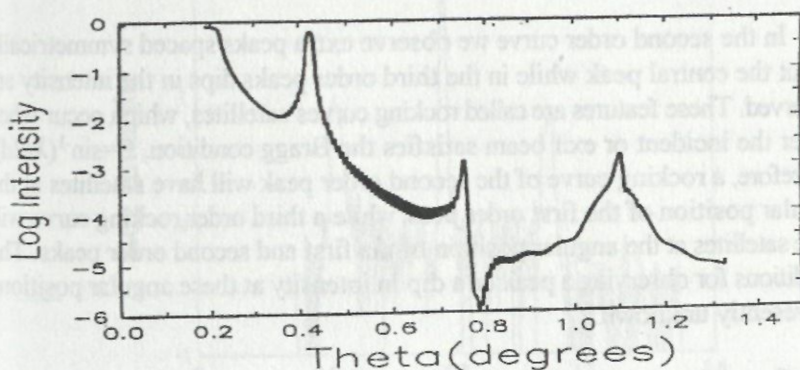

Figure 4: Model calculation for the specular reflectivity.

The lateral length scale of the vertically correlated roughness can be obtained from the rocking curves. In order to measure a rocking curve the position of the Bragg peak is found in a reflectivity measurement and the detector is set at the peak maximum with angle $2\theta_m$. The sample is then rotated from 0 to $2\theta_m$ without the sample blocking the path to the detector. This limits the lateral correlation scale that can be probed in the reciprocal space to $q_x = \pm q_z \sin\theta = \pm 2\pi / L_{max}$. For the third order peak the angular range covered is about two degrees, which corresponds to a lateral length scale down to 0.2μm. At this cutoff there still is significant diffuse intensity, implying that lateral correlation exists to a scale of less than 0.2μm. This will be demonstrated when the measurements are fitted to the theory.

Figures 5, 6 and 7 show the measured rocking curves for the first order, second order and third order peaks, respectively. The curves show two components, a sharp central peak corresponding to the specular reflection and a diffuse background. The angular range covered by the scan increases with the diffraction order as explained above. The shape of the diffuse scattering is asymmetric about the central peak because of the difference in sampling areas as the sample is rotated. The intensity of the diffuse scattering is about two orders of magnitude lower than the specular reflection, and its contribution

to the total scattering increases with increasing order.

In the second order curve we observe extra peaks spaced symmetrically about the central peak while in the third order peaks dips in the intensity are observed. These features are called rocking curves satellites, which occur when either the incident or exit beam satisfies the Bragg condition, $\theta=\sin^{-1}(\lambda/2d)$. Therefore, a rocking curve of the second order peak will have satellites at the angular position of the first order peak while a third order rocking curve will have satellites at the angular position of the first and second order peaks. The conditions for observing a peak or a dip in intensity at these angular positions is presently unknown.

Correction factors

To compare these measurements with the theory we must first correct the data to take into account the geometrical and instrumental factors that affect the measurements. These factors were estimated by Savage (1991) and include the change in beam attenuation as the incident angle changes and a geometrical effect related to the radial cut through reciprocal space when measuring a rocking curve.

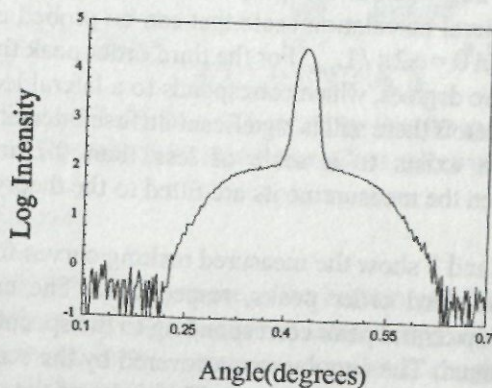

Figure 5. First order rocking curve as a function of incident angle. The curve has two components, a central specular peak and a diffuse background

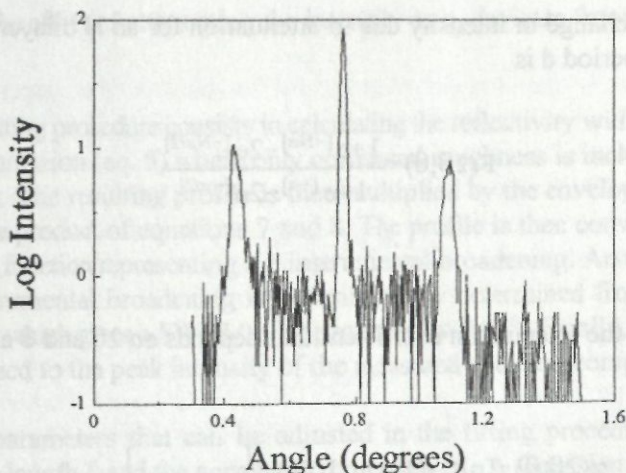

Figure 6: Second order rocking curve. Rocking curve satellites due to double diffraction are observed.

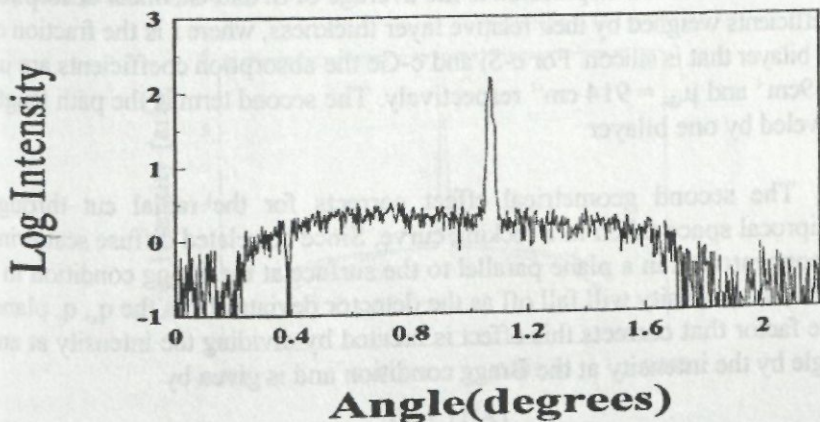

Figure 7. Third order rocking curve. The relative contribution of the diffuse component increases with diffraction order

The change in intensity due to attenuation for an N bilayer multilayer mirror of period d is

$$F(2\theta,\theta)=\frac{1+e^{[-N\alpha]}-2e^{[-N\alpha/2]}}{1+e^{[-\alpha]}-2e^{[-\alpha/2]}} \quad (6)$$

where α is the attenuation coefficient that depends on 2θ and θ and is given by

$$\alpha(2\theta,\theta)=[r\mu_{Si}+(1-r)\mu_{Ge}]\, d[\frac{1}{\sin(\theta)}+\frac{1}{\sin(2\theta-\theta)}] \quad (7)$$

The first term of this expression is the average of Si and Ge linear absorption coefficients weighed by their relative layer thickness, where r is the fraction of the bilayer that is silicon. For c-Si and c-Ge the absorption coefficients are $\mu_{Si} = 89 cm^{-1}$ and $\mu_{Ge} = 914 cm^{-1}$ respectively. The second term is the path length traveled by one bilayer.

The second geometrical effect corrects for the radial cut through reciprocal space taken in a rocking curve. Since correlated diffuse scattering is concentrated in a plane parallel to the surface at the Bragg condition in a radial, the intensity will fall off as the detector deviates from the q_x, q_y plane. The factor that corrects this effect is created by dividing the intensity at any angle by the intensity at the Bragg condition and is given by

$$G(q_z) = \frac{I[q_z(\theta_m,\theta)]}{I[q_z=q_z(Bragg)]} \quad (8)$$

which has the effect of attenuating the intensity as q_z deviates from the Bragg condition.

The fitting procedure consists in calculating the reflectivity with the single surface expression (eq. 5) where only correlated roughness is included in the calculation. The resulting profile is then multiplied by the envelope function given by the product of equations 7 and 8. The profile is then convolved with a Gaussian function representing the instrumental broadening. An upper limit to the instrumental broadening is experimentally determined from the first order peak, which gives a FWHM of approximately 0.02^{0}. Finally, the profile is normalized to the peak intensity of the measured data and compared.

The parameters that can be adjusted in the fitting procedure are the correlation length ζ and the correlated roughness σ_c. A Gaussian correlation function is always assumed, which determines the overall shape of the diffuse scattering. The ratio of the specular to diffuse intensities depends on both the correlation length and roughness while the width of the diffuse component depends primarily on the correlation length.

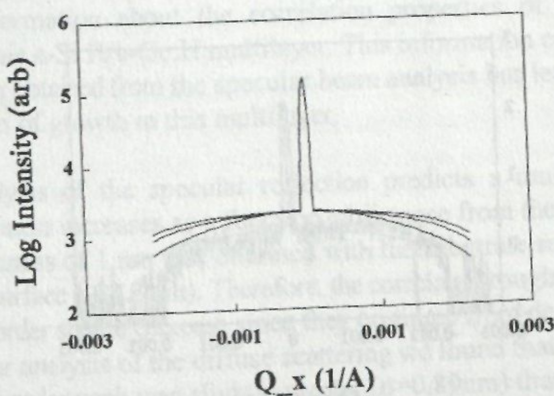

Figure 8: Range of calculated fits for the third order rocking curve as a function of the x-component of the wave vector. Top: σ_c=0.92nm, ζ=15nm; Center : σ_c=0.73nm, ζ=30nm; Bottom:σ_c=0.57nm, ζ=60 nm

Fitting results

Figure 8 shows a set of possible fits for the third order peak. The parameters for the correlated roughness range from 0.92 nm to 60 nm whereas the correlation length ranges from 15 nm to 60 nm. In order to get a bigger correlation length, the rms roughness has to decrease if we want to maintain the same peak to background intensity ratio. The best fit for the third order peak is obtained for $\sigma_c = 0.73$ nm and $\zeta = 30$ nm, as shown in figure 9. The good fit to the shape of the diffuse scattering curve, which depends on the choice of correlation function, suggests that the exponential function closely resembles the lateral correlation properties of the interface roughness. In figure 10 we present the best fit for the second order peak together with the original data. The values for the fit are $\sigma_c = 0.89$ nm and $\zeta = 30$ nm . The value for the correlation length is the same but the rms roughness is slightly higher than the first order fit. We were not successful in obtaining a reasonable fit to the first order peak with any set of parameters. There are several possible explanations for this, including the fact that for the first order peak a strong interacting or high reflectivity regime is reached in which the approximations that led to the theoretical treatment are no longer valid.

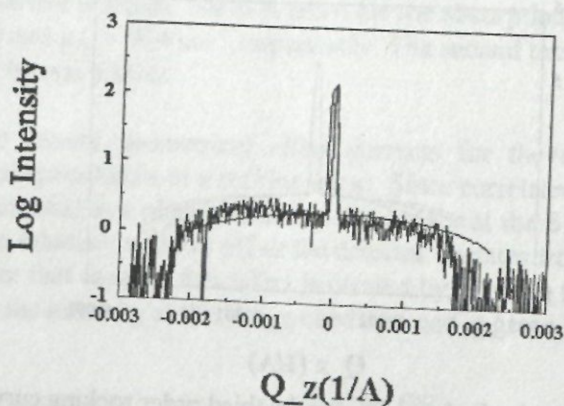

Figure 9. Best fit for the third-order rocking curve with parameters σ_c=0.73nm and ζ=30nm

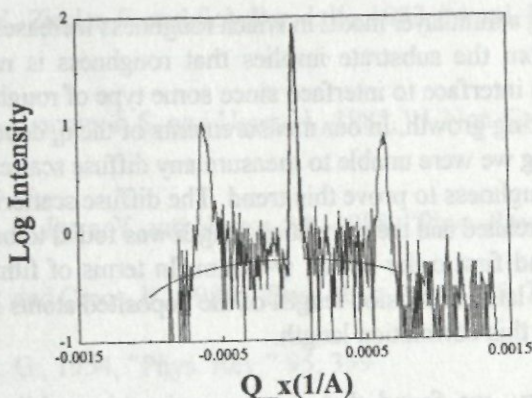

Figure 10: Theoretical fit to the second order rocking curve. The fitting parameters are σ_c=0.89nm and ζ=30nm.

Conclusions

The analysis of the diffuse part of the scattered intensity has provided important information about the correlation properties of the interface roughness in this a-Si:H/a-Ge:H multilayer. This information combined with the information obtained from the specular beam analysis has lent insight into the mechanism of growth in this multilayer.

The analysis of the specular reflection predicts a multilayer where interface roughness increases as a function of distance from the substrate. An average roughness of 1 nm was obtained with the substrate smoother (~ 0.3 nm) than the surface (~ 1.8 nm). Therefore, the correlated roughness for peaks of increasing order should decrease since they originate from deeper inside the sample. In our analysis of the diffuse scattering we found that the roughness of the second order peak was slightly greater (σ=0.89nm) than that obtained from the third order (σ=0.73nm). The fact that these values are very close and that we were able to fit only two peaks makes it difficult to establish any trend in the roughness profile as a function of depth at this time.

In addition, a multilayer model in which roughness increases as a function of distance from the substrate implies that roughness is not completely correlated from interface to interface since some type of roughness build-up has to occur during growth. In our measurements of the q_z dependence of the diffuse scattering we were unable to measure any diffuse scattering related to uncorrelated roughness to prove this trend. The diffuse scattering was found to be mostly correlated and the correlation length was found to be the same for both second and first order peaks, ζ=30nm. In terms of film growth, this suggests that the lateral diffusion length of the deposited atoms is of the order of, or less than, this correlation length.

In summary, we found that roughness in this multilayer is mostly correlated from interface to interface on the length scale given by the correlation length. The rms roughness obtained in the diffuse analysis is comparable to the average roughness obtained from the modeling of the specular reflectivity σ_c=1nm. We found no clear indication of roughness variation as a function of depth from the modeling of the diffuse scattering although the fit to the second order peak gives a bigger rms roughness than the third order peak. Further measurement and measurements on other samples are needed in order to obtain additional information. We can, for example, perform the same set of measurements with a different wavelength of x rays. This will change the penetration depth of the x rays and the Bragg peaks of the same order will originate from different depths within the sample. A direct comparison between such peaks should corroborate any variation of roughness with depth.

References

Abeles, B. And Tiedje, T., 1983, "Phys.Rev. Lett.", 51

Ehrenberg, W., 1949, "J. Opt. Soc. Am." 39, 741

Harvey, J. E., Zmek, W. P. and Moran, E. C., 1989, "SPIE" 1160, 209

Lepetre, Y., Ziegler, E. and Schuller, I. K., 1987, "Appl. Phys. Lett." 50,

Lepetre, Y., Ziegler, E. and Schuller, I. K., 1987, "Appl. Phys. Lett." 50, 1480

Maley, N., Lannin, J. S. and Ugur, H., 1985, "J. Non-Cryst. Solids" 77, 1073

Miyazaki, S., Ihara, Y. and Hirose, M., 1988, "Phys. Rev. Lett." 59, 125

Nevot, L. and Croce, P., 1980, "Rev. Phys. Appl." 15, 761

Parrat, L. G., 1954, "Phys. Rev." 95, 359

Persans, P. D., Ruppert, A.F., Abeles, B. and Tiedje, T., 1985, "Phys. Rev.", B 32, 5558

Persans, P. D., Ruppert, A. F., Wu, Y. J., Abeles, B., Lanford, W. and Pantojas, V., 1989, "Journal of Non-Cryst. Solids", 114, 771

Savage, D. E., Klein, J., Schmke, N., Phang, Y. H., Jankowski, T., Jacobs, J., Kariotis, R. and Lagally, M. G., 1991, "J. Appl. Phys." 69, 1411

Shirai, H., Tanabe, A., Hanna, J., Oda, S., Nakamura, T. and Shimizu, I., 1986, "Jpn. J. Appl. Phys.", **25**, L537

Sinha, S. K., Sorota, E. B. and Garoff, S., 1988, "Phys. Rev." B 38, 2297

Spiller, E., 1988, "Revue Phys. Appl." 23, 1687

Stearn, D. J., 1989, "J. Appl. Phys.", **65**, 491

Tsuda, S., Haku, H., Tarui, H., Matsuyama, T., Sayama, K., Nakashima, Y., Nakano, S., Ohnishi, M. and Kuwano, Y., 1987, "Mat. Res. Soc. Symp. Proc." **95**, 311

Williams, G. V. M., Bittar, A. and Trodahl, H. J., "J. Appl. Phys." 64, 5148

Wronki, C. R., Persans, P. D. and Abeles, B., 1986, "Appl. Phys. Lett." 49, 569